The XFEM for high-gradient solutions in convection-dominated problems

Safdar Abbas[1] Alaskar Alizada[2] and Thomas-Peter Fries[2] *

[1] *AICES, RWTH Aachen University, Schinkelstr. 2, 52062 Aachen, Germany*
[2] *CATS, RWTH Aachen University, Schinkelstr. 2, 52062 Aachen, Germany*

SUMMARY

Convection-dominated problems typically involve solutions with high gradients near the domain boundaries (boundary layers) or inside the domain (shocks). The approximation of such solutions by means of the standard finite element method requires stabilization in order to avoid spurious oscillations. However, accurate results may still require a mesh refinement near the high gradients. Herein, we investigate the extended finite element method (XFEM) with a new enrichment scheme that enables highly accurate results without stabilization or mesh refinement. A set of regularized Heaviside functions is used for the enrichment in the vicinity of the high gradients. Different linear and non-linear problems in one and two dimensions are considered and show the ability of the proposed enrichment to capture arbitrary high gradients in the solutions.

KEY WORDS: Extended finite element method (XFEM), high-gradient solutions, convection-diffusion, convection-dominated, boundary layers, shocks

1. Introduction

The finite element method (FEM) has been extensively used to approximate the solution of partial differential equations. The technique has been perfected in many ways for smooth solutions, however, its application to discontinuous or singular solutions is not trivial. For approximating discontinuous solutions, the element edges need to be aligned to the discontinuity. For singularities and high gradients, mesh refinement is needed. Moreover, for a moving discontinuity, re-meshing the computational domain imposes an additional computational overhead. The extended finite element method (XFEM) [1, 2] has the potential to overcome these problems and produces accurate results without aligning elements to discontinuities and without refining the mesh near singularities. These properties have made the XFEM a particularly good choice for the simulation of cracks, see e.g. [3, 4, 5, 6], as in this application, both, discontinuities (across the crack surface) and high gradients (at the crack front) are present.

*Correspondence to: fries@cats.rwth-aachen.de

In this paper, we focus on advection-dominated problems as they naturally occur in fluid dynamics and many other transport problems. For such problems, high gradients are observed near the domain boundaries (boundary layers) or inside the domain (shocks). Stabilization is typically needed in the context of the standard FEM [7, 8, 9] in order to avoid spurious oscillations. However, even with stabilization, high gradients are often still not represented sufficiently accurate on coarse meshes and mesh refinement is still needed in addition.

We employ the XFEM with the aim to approximate convection-dominated problems without stabilization or mesh refinement. A new enrichment scheme is proposed that enables the approximation to capture arbitrary high gradients. We want to avoid an adaptive procedure which determines *one* suitable enrichment function through an iterative procedure which then needs to be realized within each time-step. In contrast, we rather provide a set of enrichment functions near the largest gradient (i.e. along the boundary or near a shock). This set is based on regularized Heaviside functions and is able to treat all gradients starting from the gradient that can no longer be represented well by the standard FEM approximation up to the case of almost a jump. It is noted that in the presence of diffusion, no matter how small, true jumps in the solutions are impossible and the use of the step enrichment, being standard in many applications of the XFEM, is not allowed (due to considerations from functional analysis) for the problems considered here.

The use of regularized step functions in the XFEM has been realized in the simulation of cohesive cracks and shear bands: Patzák and Jirásek [10] employed regularized Heaviside functions for resolving highly localized strains in narrow damage process zones of quasibrittle materials. Thereby, they incorporate the non-smooth behavior in the approximation space. Arieas and Belytschko [11] embedded a fine scale displacement field with a high strain gradient around a shear band. They used a tangent hyperbolic type function for the enrichment. Benvenuti [12] also used a similar function for simulating the embedded cohesive interfaces. Waisman and Belytschko [13] proposed a parametric adaptive strategy for capturing high gradient solutions. One enrichment function is designed to match the qualitative behavior of the exact solution with a free parameter. The free parameter is optimized by using *a-posteriori* error estimates.

In [10, 11, 12], the regularized Heaviside functions depend on physical considerations. Only *one* enrichment function is used in [11, 13]. A common feature of most previous applications is that the change from 0 to 1 takes place within one element. Herein, however, we show that for arbitrary high gradients in convection-dominated problems, the length scale where the change from 0 to 1 takes place should exceed the element size and, consequently, extends to several elements around the largest gradient. Furthermore, it is found that only one enrichment function cannot cover the complete range of gradients and that a set of enrichment functions is needed. The fact that several enrichment functions are present and some of them extend over several elements complicates the implementation of the XFEM compared to standard XFEM applications.

The paper is organized as follows. The general form of XFEM-approximations for multiple enrichment terms is given in Section 2. The governing equations for the considered linear and non-linear convection-dominated problems are described in Section 3. In Section 4, the enrichment scheme for the XFEM is proposed for high gradients inside the domain. The procedure for finding suitable sets of enrichment functions is discussed and additional issues such as the quadrature and the removal of almost linearly dependent degrees of freedom are mentioned. Several numerical results are presented which obtain highly accurate results

without stabilization and mesh refinement. Section 5 gives the enrichment functions that are useful in order to capture high gradients near the boundaries. Again, numerical results show the success of the enrichment scheme. The paper concludes with a summary and outlook in Section 6.

2. XFEM formulation

A standard XFEM approximation of a scalar function $u^h(\boldsymbol{x})$ in a d-dimensional domain $\Omega \in \mathbb{R}^d$ is given as

$$u^h(\boldsymbol{x},t) = \underbrace{\sum_{i\in I} N_i(\boldsymbol{x}) u_i}_{\text{strd. FE part}} \; + \; \underbrace{\sum_{i\in I^\star} N_i^\star(\boldsymbol{x}) \cdot \psi(\boldsymbol{x},t)\; a_i}_{\text{enrichment}}, \tag{2.1}$$

for the case of only one enrichment term. $N_i(\boldsymbol{x})$ is the standard FE function for node i, u_i is the unknown of the standard FE part at node i, I is the set of all nodes in the domain, $N_i^\star(\boldsymbol{x})$ is a partition of unity function of node i, $\psi(\boldsymbol{x},t)$ is the global enrichment function, a_i is the unknown of the enrichment at node i, and $I^\star$ is a nodal subset of enriched nodes. The functions $N_i^\star(\boldsymbol{x})$ equal $N_i(\boldsymbol{x})$ in this work although this is not necessarily the case. The global enrichment function $\psi(\boldsymbol{x},t)$ incorporates the known solution characteristics into the approximation space and is time-dependent in this work. The XFEM is generally used to approximate discontinuous solutions (strong discontinuities) or solutions having discontinuous derivatives (weak discontinuities). Then, typical choices for the enrichment functions are: The step-enrichment

$$\psi(\boldsymbol{x},t) = \operatorname{sign}(\phi(\boldsymbol{x},t)) = \begin{cases} -1 : \phi(\boldsymbol{x},t) < 0, \\ \;\;0 : \phi(\boldsymbol{x},t) = 0, \\ \;\;1 : \phi(\boldsymbol{x},t) > 0, \end{cases} \tag{2.2}$$

for strong discontinuities (jumps) and the abs-enrichment

$$\psi(\boldsymbol{x},t) = \operatorname{abs}(\phi(\boldsymbol{x},t)) = |\phi(\boldsymbol{x},t)|. \tag{2.3}$$

for weak discontinuities (kinks).

It is noted that these enrichment functions depend on the level-set function $\phi(\boldsymbol{x},t)$ which is typically the signed-distance function. Assuming that $\phi_d(\boldsymbol{x},t)$ is the shortest distance at time t of every point $\boldsymbol{x}$ in the domain to the (moving) discontinuity, then

$$\phi(\boldsymbol{x},t) = \begin{cases} -\phi_d(\boldsymbol{x},t) & \forall \boldsymbol{x} \in \Omega^-, \\ +\phi_d(\boldsymbol{x},t) & \forall \boldsymbol{x} \in \Omega^+, \end{cases} \tag{2.4}$$

where Ω^- and Ω^+ are the two subdomains on the opposite sides of the interface. See [14, 15] for further details on the level-set method.

Let us now adapt the XFEM approximation and level-set concept for the situation relevant for convection-dominated problems. The level-set function is used to describe the position of the largest gradient, i.e. the position of the shock, inside the domain. It is assumed that this position is known in the initial situation (at time $t = 0$). However, the development of the position of the largest gradient (the shock) in time is typically not known and not needed for

the proposed technique. Instead, an additional transport equation for the level-set function is solved which appropriately accounts for the movement in time; this shall be seen in more detail later. For large gradients near the boundary, i.e. for boundary layers, the position of the largest gradient is directly the boundary itself, so that the level-set concept is not needed then. The enrichment functions for boundary layers depend only on the discretization near the wall.

As mentioned above, several enrichment functions are needed in order to capture arbitrary high gradients in convection-dominated problems. Therefore, the XFEM-approximation (2.1) is extended in a straightforward manner as

$$u^h(\boldsymbol{x},t) = \sum_{i\in I} N_i(\boldsymbol{x})u_i \;\; + \;\; \sum_{j=1}^{m}\sum_{i\in I_j^\star} N_i^\star(\boldsymbol{x})\cdot\psi_j(\boldsymbol{x},t)\; a_i^j, \tag{2.5}$$

where m is the number of enrichment terms. It is noted that each enrichment function $\psi_j(\boldsymbol{x},t)$ may refer to a different set of enriched nodes $I_j^\star$.

3. Governing equations

In this work, numerical results will be presented individually in sections 4 and 5 for solutions with high gradients inside the domain and at the boundary, respectively. Therefore, it proves useful to define the governing equations of the considered advection-diffusion problems beforehand. Linear and non-linear advection-diffusion problems are considered in one and two dimensions.

3.1. Linear advection-diffusion equation

Let Ω be an open, bounded region in $\Omega\in\mathbb{R}^d$. The boundary is denoted by Γ and is assumed smooth. The linear advection-diffusion problem with prescribed constant velocities $\boldsymbol{c}\in\mathbb{R}^d$ and a constant, scalar diffusion parameter $\kappa\in\mathbb{R}$ is stated in the following initial/boundary value problem: Find $u(\boldsymbol{x},t)\;\forall\boldsymbol{x}\in\bar{\Omega}$ and $\forall t\in[0,T]$ such that

$$\dot{u}(\boldsymbol{x},t) \;=\; -\boldsymbol{c}\cdot\nabla u + \kappa\cdot\Delta u, \quad \text{in } \Omega\times\,]0,T[, \tag{3.1}$$

$$u(\boldsymbol{x},0) \;=\; u_0(\boldsymbol{x}), \quad \forall\boldsymbol{x}\in\Omega \tag{3.2}$$

$$u(\boldsymbol{x},t) \;=\; \hat{u}(\boldsymbol{x},t), \quad \forall\boldsymbol{x}\in\Gamma\times\,]0,T[, \tag{3.3}$$

where $\Delta u = \nabla\cdot(\nabla u)$ and $\dot{u} = \partial u/\partial t$. The initial condition $u_0:\Omega\to\mathbb{R}$ and Dirichlet boundary condition $\hat{u}:\Gamma\times]0,T[\to\mathbb{R}$ are prescribed data. No Neumann boundary conditions are considered.

For the approximation with finite elements, the problem has to be stated in its discretized variational form. The variational form also depends on the time-discretization: If the derivative in time is treated by finite differences the test and trial function spaces are

$$\mathcal{S}^h_{\mathrm{TS}} \;=\; \left\{u^h\in H^{1h}(\Omega)\mid u^h=\hat{u}^h \;\text{ on }\; \Gamma\right\}, \tag{3.4}$$

$$\mathcal{V}^h_{\mathrm{TS}} \;=\; \left\{w^h\in H^{1h}(\Omega)\mid w^h=0 \;\text{ on }\; \Gamma\right\}, \tag{3.5}$$

where "TS" stands for "time stepping". H^{1h} is a finite dimensional subspace of the space of square-integrable functions with square-integrable first derivatives H^1. H^{1h} is spanned by

the standard finite element and enrichment functions given in the approximation (2.5). The objective is to find $u^h \in \mathcal{S}^h_{\rm TS}$, such that $\forall w^h \in \mathcal{V}^h_{\rm TS}$:

$$\int_\Omega w^h \left(\dot{u}^h + \boldsymbol{c}\cdot\nabla u^h\right) d\Omega + \kappa \int_\Omega \nabla w^h \cdot \nabla u^h d\Omega = 0\,. \tag{3.6}$$

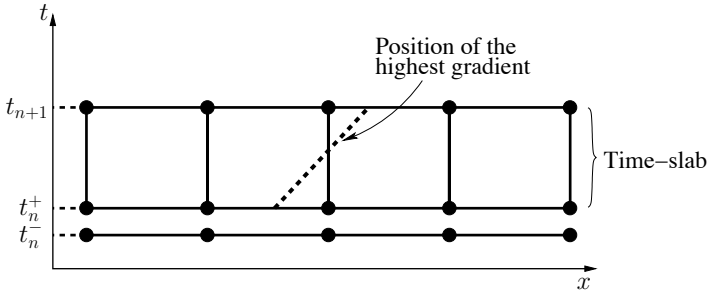

Figure 1. Space-time discretization for the discontinuous Galerkin method in time.

In this work, we also consider the discontinuous Galerkin method in time for the time-discretization, see e.g. [9]. The space-time domain $Q = \Omega\times]0,T[$ is divided into time slabs $Q_n = \Omega\times]t_n, t_{n+1}[$, where $0 = t_0 < t_1 < \ldots < t_{\rm N} = T$. Each time slab is discretized by extended space-time finite elements, see Figure 1. The enriched approximation is of the form (2.5), however, the finite element functions are now also time-dependent, i.e. $N_i(\boldsymbol{x},t)$ and $N_i^\star(\boldsymbol{x},t)$. The test and trial function spaces are

$$\mathcal{S}^h_{\rm ST} = \left\{u^h \in H^{1h}(Q_n) \mid u^h = \hat{u}^h \ \text{ on } \ \Gamma\times]t_n, t_{n+1}[\right\}, \tag{3.7}$$

$$\mathcal{V}^h_{\rm ST} = \left\{w^h \in H^{1h}(Q_n) \mid w^h = 0 \ \text{ on } \ \Gamma\times]t_n, t_{n+1}[\right\}, \tag{3.8}$$

and are again spanned by the FE shape functions and enrichment functions in (2.5). "ST" stands for "space-time". The discretized weak form may be formulated as follows: Given $\left(u^h\right)_n^-$, find $u^h \in \mathcal{S}^h_{\rm ST}$ such that $\forall w^h \in \mathcal{V}^h_{\rm ST}$

$$\int_{Q_n} w^h \left(\dot{u}^h + \boldsymbol{c}\cdot\nabla u^h\right) dQ + \kappa \int_{Q_n} \nabla w^h \cdot \nabla u^h dQ, \tag{3.9}$$

$$+ \int_{\Omega_n} \left(w^h\right)_n^+ \cdot \left(\left(u^h\right)_n^+ - \left(u^h\right)_n^-\right) d\Omega \quad = 0 \quad , \tag{3.10}$$

where $\left(u^h\right)_n^\pm$ is

$$\left(u^h\right)_n^\pm = \lim_{\varepsilon\to 0} u^h\left(x, t_n \pm \varepsilon\right). \tag{3.11}$$

The continuity of the field variables is weakly enforced across the time-slabs, see (3.10). The initial condition u_0^h is set for $\left(u^h\right)_0^-$.

It is noted that Equation (3.6) on the one hand and Equations (3.9) and (3.10) on the other hand are both Bubnov-Galerkin weighted residual formulations. That is, no stabilization terms are present. The results obtained by the unstabilized XFEM approximations are compared

lateron with both stabilized and unstabilized standard FEM approximations. Stabilized weak forms in the context of the standard FEM are e.g. found in [7, 8, 16].

Remark. In order to consider for moving interfaces in the domain, a pure advection equation has to be solved in Ω for the level-set function $\phi(\boldsymbol{x}, t)$ [14, 15]. The strong form equals Equation (3.1) to (3.3) with $\kappa = 0$ and boundary conditions are only applied at the inflow.

3.2. Burgers equation

The Burgers equation in one dimension with a constant, scalar diffusion parameter $\kappa \in \mathbb{R}$ is stated in the following initial/boundary value problem: Find $u(x,t)$ $\forall x \in \bar{\Omega}$ and $\forall t \in [0,T]$ such that

$$\begin{aligned} \dot{u}(x,t) &= -u \cdot \frac{\partial u}{\partial x} + \kappa \cdot \frac{\partial^2 u}{\partial x^2}, \quad \text{in } \Omega \times]0,T[, && (3.12)\\ u(x,0) &= u_0(x), \quad \forall x \in \Omega && (3.13)\\ u(x,t) &= \hat{u}(x,t), \quad \forall x \in \Gamma \times]0,T[, && (3.14) \end{aligned}$$

The initial condition u_0 and Dirichlet boundary condition $\hat{u}$ are prescribed data. No Neumann boundary conditions are considered.

The variational form for a finite difference treatment of the temporal derivative is to find $u^h \in \mathcal{S}^h_{\mathrm{TS}}$, such that $\forall w^h \in \mathcal{V}^h_{\mathrm{TS}}$:

$$\int_\Omega w^h \left(\dot{u}^h + u^h \cdot \frac{\partial u^h}{\partial x} \right) d\Omega + \kappa \int_\Omega \frac{\partial w^h}{\partial x} \cdot \frac{\partial u^h}{\partial x} d\Omega = 0, \tag{3.15}$$

and for the discontinuous Galerkin method in time: Given $\left(u^h\right)^-_n$, find $u^h \in \mathcal{S}^h_{\mathrm{ST}}$ such that $\forall w^h \in \mathcal{V}^h_{\mathrm{ST}}$

$$\begin{aligned} \int_{Q_n} w^h \left(\dot{u}^h + u^h \cdot \frac{\partial u^h}{\partial x} \right) dQ + \kappa \int_{Q_n} \frac{\partial w^h}{\partial x} \cdot \frac{\partial u^h}{\partial x} dQ, && (3.16)\\ + \int_{\Omega_n} \left(w^h\right)^+_n \cdot \left(\left(u^h\right)^+_n - \left(u^h\right)^-_n \right) d\Omega \quad = 0 \quad . && (3.17) \end{aligned}$$

4. XFEM for high gradients *inside* the domain (shocks)

In the following, an overview over existing regularized step functions is given. A particular suitable choice for high gradients inside the domain is discussed. The next step is to define a *set* of these functions in order to capture arbitrary gradients. An optimization procedure is described which is used to determine sets of 3, 5, and 7 enrichment functions.

4.1. Different classes of regularized step functions

In this work, a minimum requirement of a regularized step function that can be used as an enrichment function for high gradients in the domain is that they depend on the level-set function $\phi(\boldsymbol{x}, t)$. The zero-level of $\phi(\boldsymbol{x}, t)$ is the centerline of the highest gradient (shock). Furthermore, we need control over the gradient of the regularized step function. This can

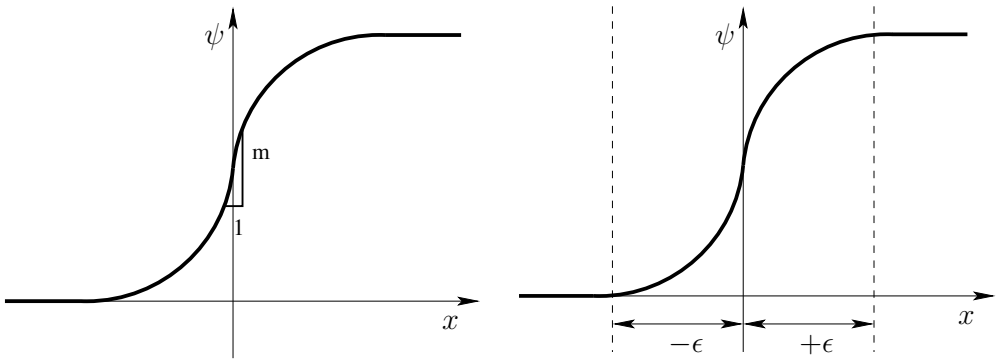

Figure 2. Regularized Heaviside function for a high gradient enrichment: (a) the gradient is scaled directly, (b) the gradient is scaled indirectly by controlling the width.

be a parameter that directly scales the gradient, see Fig. 2(a), or which controls the gradient indirectly by prescribing the length-scale where the change from 0 to 1 takes place, see Fig. 2(b).

Three different choices of enrichment functions are investigated. The first function is adapted from Areias and Belytschko [11] and depends on a parameter ϵ that specifies the width of the function and a parameter n that specifies the gradient of the function. By "width" of the regularized step function we refer to the region where the function varies monotonically between 0 (or -1) and 1. The higher the value of n, the steeper will be the function for the same width ϵ.

$$\psi(\phi(\boldsymbol{x},t),\epsilon,n) = \begin{cases} -1, & \text{if } \phi(\boldsymbol{x},t) < -\epsilon, \\ \dfrac{\tanh(n\phi(\boldsymbol{x},t))}{\tanh(n\epsilon)}, & \text{if } |\phi(\boldsymbol{x},t)| \leqslant \epsilon, \\ 1, & \text{if } \phi(\boldsymbol{x},t) > \epsilon. \end{cases} \tag{4.1}$$

The second function is taken from Benvenuti [12]. This function also depends on two parameters ϵ and n. The lower the value of n, the steeper will be the function for the same width ϵ.

$$\psi(\phi,\epsilon,n) = \begin{cases} -1, & \text{if } \phi < -\epsilon, \\ \text{sign}(\phi)\Big(1 - exp(\frac{-|\phi|}{n})\Big), & \text{if } |\phi| \leqslant \epsilon, \\ 1, & \text{if } \phi > \epsilon. \end{cases} \tag{4.2}$$

Both of the above-mentioned functions are C^∞-continuous in the domain except at $\Gamma_\epsilon = \{\boldsymbol{x} \in \Omega : |\phi(\boldsymbol{x},t)| = \epsilon\}$ where they are C^0-continuous only, i.e. there is a kink at Γ_ϵ. This may complicate the numerical integration and artificial weak discontinuities are introduced. Consequently, for the applications considered herein it is desirable to have functions that are more than C^0-continuous in the overall domain.

The third function is a regularized Heaviside function taken from Patzák and Jirásek [10]. This function only depends on one parameter ϵ that controls the width of the function directly.

The smaller the value of ϵ, the larger is the gradient of the function

$$\psi(\phi,\epsilon) = \begin{cases} 0, & \text{if } \phi < -\epsilon, \\ \dfrac{315}{256\epsilon}\displaystyle\int_{-\epsilon}^{\phi}\left(1-\frac{\xi^2}{\epsilon^2}\right)^4 d\xi, & \text{if } |\phi| \leqslant \epsilon, \\ 1, & \text{if } \phi > \epsilon. \end{cases} \tag{4.3}$$

Evaluating the integral involved in (4.3) gives

$$\psi(\phi,\epsilon) = \frac{1}{256\epsilon^9}\left(128\epsilon^9 + 315\phi\epsilon^8 - 420\phi^3\epsilon^6 + 378\phi^5\epsilon^4 - 180\phi^7\epsilon^2 + 35\phi^9\right) \tag{4.4}$$

for $|\phi(\boldsymbol{x},t)| \leqslant \epsilon$. Definition (4.3) is C^∞-continuous in the domain, except at Γ_ϵ where it is C^4-continuous (compared to C^0-continuity of the above definitions). Therefore, we prefer (4.3) over (4.1) and (4.2) and use it throughout the remaining of this work.

It is important to note that the width ϵ should depend on the element size h of the mesh. A constant width could lead to situations where $\epsilon \gg h$, and the resulting enrichment functions would not span a good basis (i.e. the condition number would increase prohibitively). The fact that the width depends on the discretization rather than on physical considerations is in contrast to previous applications of regularized step functions in the frame of cohesive cracks and shear bands.

4.2. Optimal set of enrichment functions

The aim is to cover the complete range of high gradients starting from the gradient that can no longer be represented well by the standard FEM approximation up to the case of almost a jump (the gradient is then extremely large). For that purpose, one enrichment function is not sufficient. In contrast, several enrichment functions have to be chosen.

For a given number m of enrichment functions $\boldsymbol{\psi} = \{\psi_1(\phi,\epsilon_1),\ldots,\psi_m(\phi,\epsilon_m)\}$, an optimization procedure is employed in order to determine the corresponding values $\epsilon_1,\ldots,\epsilon_m$. The aim is to minimize the largest pointwise error

$$\varepsilon(\boldsymbol{\psi}) = \sup(u^h(x) - f(x)) \qquad \forall x \in \Omega \tag{4.5}$$

of the following interpolation problem

$$\int_\Omega w^h\ u^h(x) = \int_\Omega w^h\ f(x) \qquad \text{in } \Omega \tag{4.6}$$

where $f(x)$ is a given regularized step function that shall be interpolated by the m (enrichment) functions of (4.3), i.e.

$$u^h(x) = \sum_{j=1}^{m} \psi_j(\phi,\epsilon_j). \tag{4.7}$$

The domain is $\Omega =]0,1[$ and $\phi = x - 0.5$ is a time-independent level-set function, whose zero-level is at $x = 0.5$, i.e. where the gradient of $f(x)$ is maximum. An important point is that for each prescribed set of enrichment functions $\boldsymbol{\psi}$ (which here are regular interpolation functions), different regularized step functions for $f(\boldsymbol{x})$ are chosen and their gradients are varied systematically between a minimum and maximum gradient. For each set $\boldsymbol{\psi}$, the largest value

(a) Set of 3 enrichment functions

Enrichment Function	ϵ/h
ψ_1	2.5
ψ_2	0.27
ψ_3	0.0225

(b) Set of 5 enrichment functions

Enrichment Function	ϵ/h
ψ_1	2.5
ψ_2	0.85
ψ_3	0.265
ψ_4	0.085
ψ_5	0.0225

(c) Set of 7 enrichment functions

Enrichment Function	ϵ/h
ψ_1	2.5
ψ_2	1.5
ψ_3	0.5
ψ_4	0.25
ψ_5	0.125
ψ_6	0.0625
ψ_7	0.0225

Table I. Optimal sets of enrichment functions, h is a characteristic element size near the shock.

for ε is stored in $\varepsilon_{\text{total}}$. The optimal set for each number m is then the one with the smallest $\varepsilon_{\text{total}}$. In this way, optimal sets are found for three, five and seven enrichment functions. A graphical representation of these sets is given in Figures 3(a)-3(c).

The next step is to use this set of functions within an XFEM approximation of the form (2.5). The functions have to be scaled with respect to the element size. Therefore, the resulting widths $\epsilon_1, \cdots \epsilon_m$ in table I depend on h. It is seen that some of these functions vary between 0 and 1 over more than one element. For a given enrichment function ψ_j, it is important to enrich the nodes (through the choice of $I_j^\star$) of all elements where ψ_j varies between 0 and 1. The appropriate nodes are easily determined by means of the value of the level-set function at each node which is directly the distance to the shock. It is noted that in standard XFEM applications, where the step- and abs-enrichment of Equations (2.2) and (2.3) is used, only the nodes of elements that are crossed by the zero-level of ϕ are enriched, i.e. in $I^\star$.

In the following, all results are obtained for the set of *seven* enrichment functions. It is important to recall that these widths are relative to the element sizes near the shock. That is, the widths decrease with mesh refinement and vice versa.

4.3. Quadrature

In the case of XFEM approximations with discontinuous enrichments, elements are subdivided into sub-cells for integration purposes [2]. For continuous enrichment functions as used in this work, this subdivision is not necessarily required. However, due to the high gradients of the enrichment functions inside the element, a large number of integration points may be needed for accurate quadrature.

It is well-known that Gauss quadrature rules concentrate integration points near the element edges, see Figure 4(a) for the example of three quadrilateral elements. It is desirable to

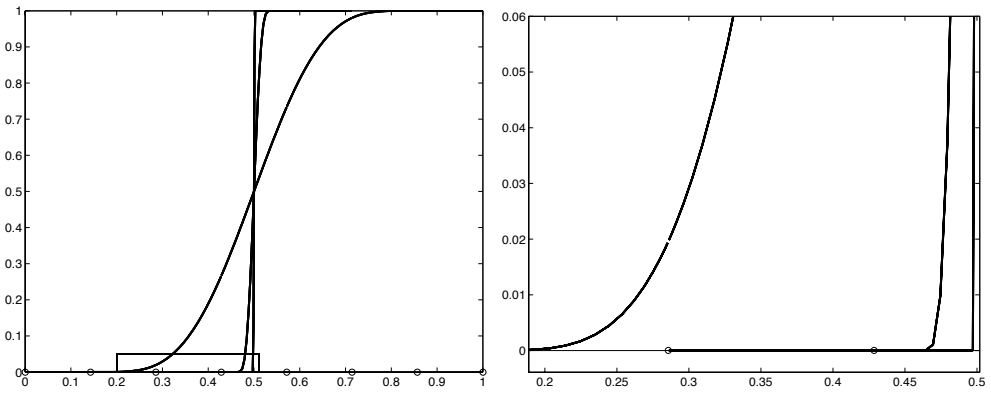

(a) Optimal set of three enrichment functions

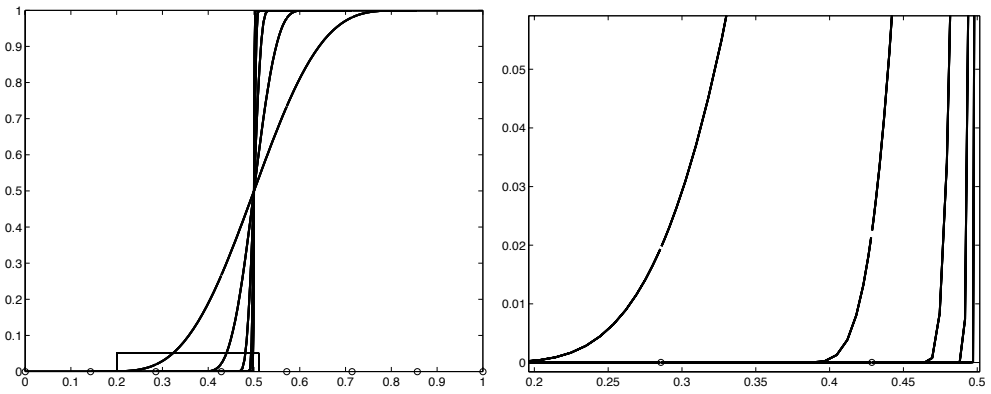

(b) Optimal set of five enrichment functions

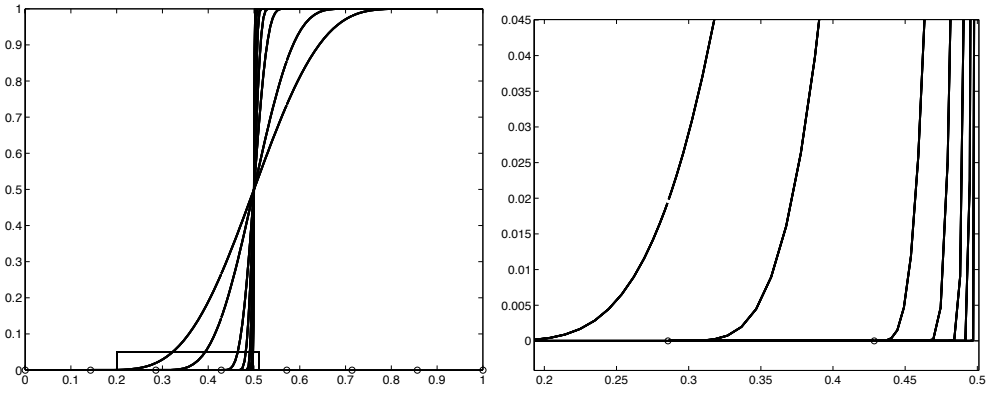

(c) Optimal set of seven enrichment functions

Figure 3. Optimal sets of enrichment functions. The boxes in the left figures show the regions which are zoomed out in the right figures.

concentrate integration points near the shock where the enrichment functions have high gradients, too. Therefore, we found that a subdivision as known from most XFEM applications with discontinuous enrichments is also advantageous for the high gradient enrichments proposed herein. This is confirmed in a number of studies and it is found that, for a given level of accuracy of the quadrature, less integration points are needed for the decomposition into integration subcells than without. An example of the resulting integration points is given in Figure 4(b) where the thick dashed line shows the position of the highest gradient in the two-dimensional domain. It can be seen that the density of the integration points is large near the shock as desired. More advanced quadrature schemes for high gradient integrands are discussed e.g. in [17, 11, 18] and are not in the focus of this work.

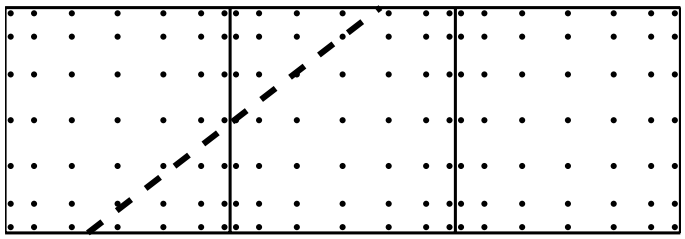

(a)

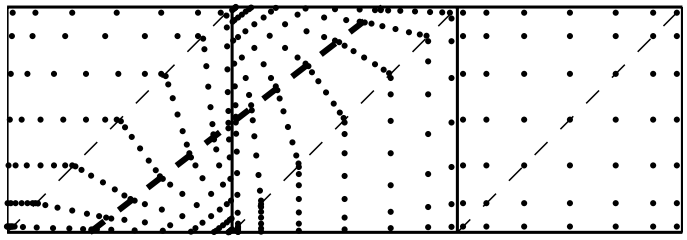

(b)

Figure 4. Integration points in quadrilateral elements, (a) without partitioning, (b) with partitioning with respect to the position of the highest gradient.

4.4. Blocking of some enriched degrees of freedom

In the case of discontinuous functions, only the nodes of cut elements are enriched with a step function. It is then well-known that if the difference of the element areas/volumes on the two sides of the interface is increasingly large, then the enrichment becomes more and more linearly dependent [19, 20]. It is then useful to remove those degrees of freedom whose contribution to the overall system of equations is negligible. This can be called "blocking" degrees of freedom.

The situation is similar for the proposed enrichment scheme for high gradient solutions inside the domain. We found that a simple procedure for the blocking can be used for the test cases considered in this work: Once the final system matrix is assembled, the absolute maximum value of each row of the enriched degrees of freedom is determined. If this value is less than

a specific tolerance, e.g. 10^{-7}, the corresponding degree of freedom is blocked. In this way, without affecting the accuracy of the approximation noticeably, the conditioning of the system remains within a reasonable threshold.

4.5. Numerical examples with high gradients inside the domain

Four in-stationary convection-dominated problems are considered in order to show the effectiveness of the enrichment scheme. The optimal set of seven enrichment functions described in section 4.2 is used to enrich the approximation space. The position of the highest gradient is represented by the zero-level of a level-set function.

4.5.1. Burgers equation with stationary high gradient developing over time The Burgers equation in one dimension is considered first, see section 3.2 for the governing equations. The domain is $\Omega =]0, 1[$ and $T = 1$. The initial condition is given as $u_0(x) = \sin 2\pi(x)$. In this setting, the gradient at $x = 0.5$ increases over time withough changing the position of the highest gradient in Ω. The maximum gradient over time depends on the diffusion coefficient κ, and, as long as $\kappa > 0$, the gradient is finite. However, for small diffusion coefficients very high gradients develop at $x = 0.5$. Herein, κ is chosen as 1.25×10^{-3}. The temporal discretization is achieved through the Crank-Nicolson method where $\dot{u} = F(u, t)$ is replaced by

$$\frac{u^{n+1} - u^n}{\triangle t} = \frac{1}{2}\big(F(u^{n+1}, t^{n+1}) + F(u^n, t^n)\big) \tag{4.8}$$

Consequently, the variational form (3.15) applies. The nonlinear term $u \cdot u_{,x}$ is linearized by the Newton-Raphson method.

Linear finite element shape functions are used for $N_i(x)$ and $N_i^\star(x)$ in the XFEM approximation (2.5). The mesh consists of an even number of equally-spaced nodes. Thus, the highest gradient at $x = 0.5$ is always present in the middle of the center element. The initial position of the highest gradient is known and does not change during the computation. Therefore, the level-set function, $\phi(x) = x - 0.5$, does not change in time and all enrichment functions are time-independent. Then, time-stepping methods such as the Crank-Nicolson method can be used in the standard way. It is noted that for *moving* high gradients, the enrichment functions are time-dependent which effects the time discretization. Time-stepping schemes are then to be used with care as discussed in [21, 22]. Consequently, for all subsequent test-cases with moving high gradients we employ the discontinuous Galerkin method in time (i.e. space-time elements).

Figure 5(a) shows the results obtained by the standard FEM without using stabilization or refinement, based on a mesh with 21 linear elements (22 degrees of freedom) and 20 time-steps. Solutions at some intermediate time steps are shown and the exact solution at the final time T is shown by a thick, gray line. Large oscillations are observed in the FEM solution as expected. When solving the SUPG-stabilized weak form of this problem, see e.g. [7], the oscillations are considerably reduced but the accuracy is still low, see figure 5(b). The XFEM results on the same mesh without stabilization are shown in Figure 5(c). The approximation space is enriched by the set of seven enrichment functions resulting in 42 degrees of freedom of the overall enriched approximation. No oscillations are visible in the XFEM solution.

Figure 6 compares the XFEM and FEM solutions in terms of the error in the L_2-Norm

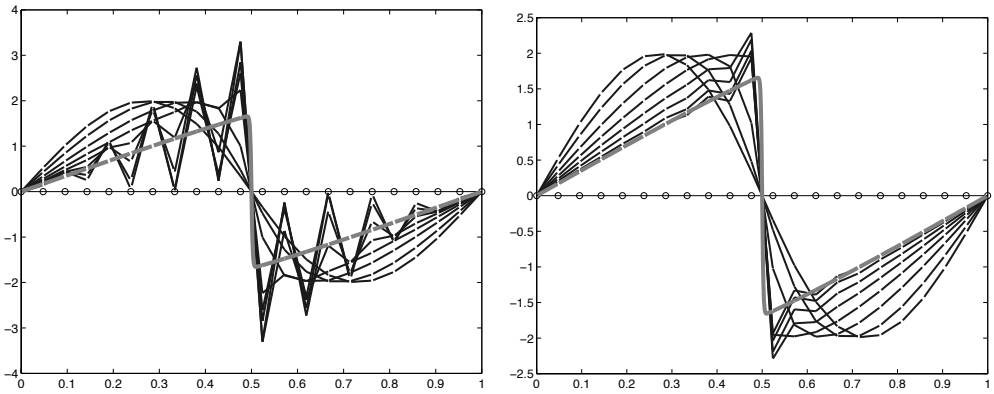

(a) Unstabilized FEM results.

(b) FEM results with SUPG stabilization.

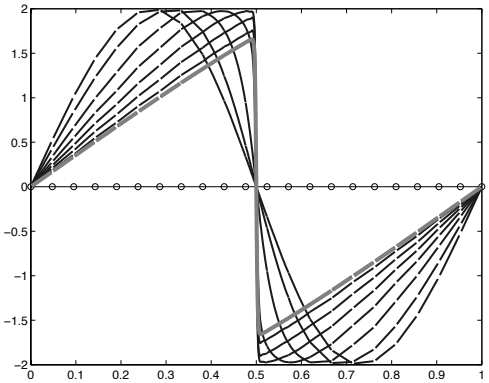

(c) Unstabilized XFEM results.

Figure 5. Results for the 1D Burgers Equation.

which is computed in the spatial domain at the final time level $t = T$ as

$$e = \frac{\sqrt{\int_\Omega (u^{ex}(x,T) - u^h(x,T))^2 d\Omega}}{\sqrt{\int_\Omega (u^{ex}(x,T))^2 d\Omega}} \tag{4.9}$$

where u^{ex} is the exact solution (which is known for this setting) and u^h is the approximation. It is seen that the accuracy of the XFEM approximation is much better for coarse meshes when compared to the standard finite element approximation. The down-peaks in the convergence plot for the XFEM approximation on coarse meshes come from situations where the gradient of the exact solution coincides better with one of the enrichment functions. Rather than these coincidental interferences of the discretization, enrichment, and the exact solution, the true benefit is the improvement of the error and the absence of oscillations on all coarse meshes. With mesh refinement, both methods obtain the same asymptotic convergence rate of 2. The improvement due to the enrichment is lost on highly refined meshes that are able to reproduce

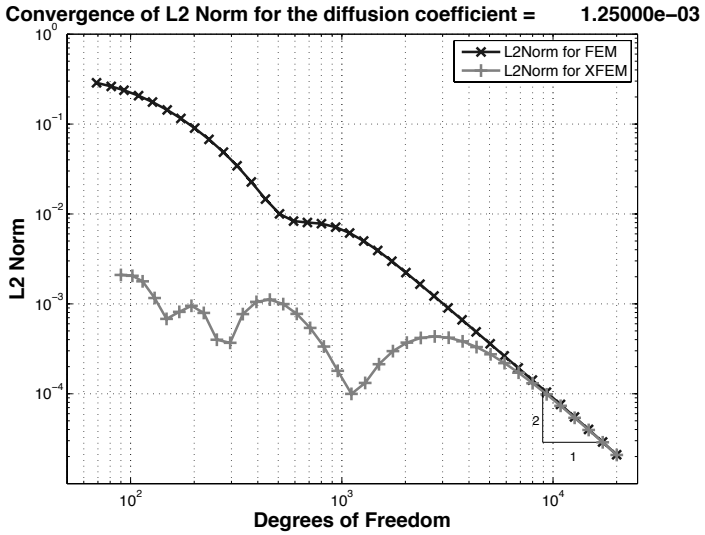

Figure 6. Convergence in the L_2-norm for a diffusion coefficient of $\kappa = 1.25 \cdot 10^{-3}$.

the large gradient in the exact solution sufficiently accurate. In this case, the enrichment is obviously not needed.

We conclude that through the proposed enrichment scheme, oscillations in the high gradient solution can be removed and the solution quality can be improved without refining the mesh and/or using stabilization.

4.5.2. Advection-diffusion equation with moving high gradient (position known a priori) The second test-case is a convection-dominated linear transport problem in one dimension. The governing equations are given in section 3.1. In this case, the position of the highest gradient is moving with a given velocity through the domain. In the considered linear transport problem, shocks may not develop in time as in the previous example. Therefore, a high gradient is already prescribed in the initial condition and is then transported in Ω. We specify the parameters of the governing equations as $\Omega =]0, 1[$, $c = 5$, $\kappa = 10^{-6}$, $T = 0.055$ and $u_0(x) = -2 \cdot \psi(\phi, 0.5, 1500)$ with ψ of Equation (4.1).

The movement of the interface is reflected by solving a transport problem for the level-set function, see Section 3.1. In this test case, the transport of the level-set function does not depend on the solution of the advection-diffusion problem for u so that it may be solved in advance. Due to the movement of the interface, we prefer to employ the discontinuous Galerkin method in time so that the variational weak form (3.9) is relevant. The movement of the high gradient is then captured naturally [21, 22].

The unstabilized results obtained with the FEM using 21 linear elements and 20 time-steps are shown in Figure 7(a). These results show large oscillations near the high gradient. Again, the situation can be improved with stabilization, however, the high gradient is then smoothed out due to diffusive effects. In contrast, the XFEM results are highly accurate and show no

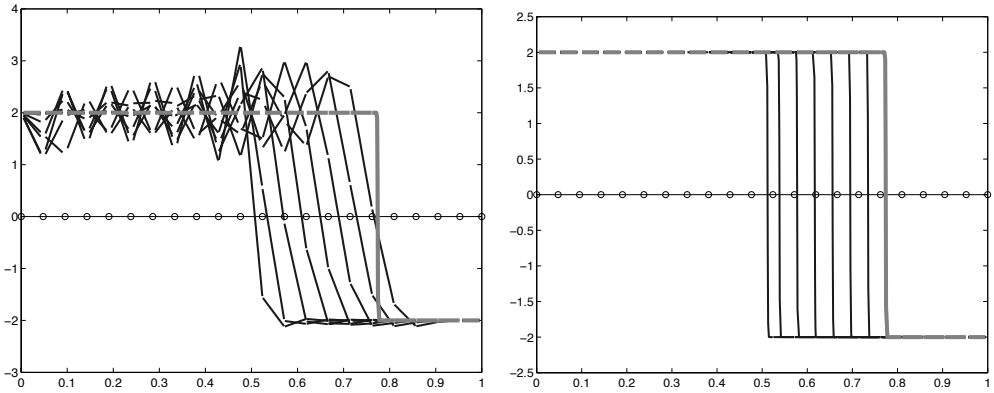

(a) FEM results. (b) XFEM results.

Figure 7. Unstabilized results for the linear advection-diffusion equation in one dimension.

oscillations even without stabilization, see Figure 7(b).

We conclude that it is possible to get highly accurate, non-oscillatory results for a moving high gradient solution without stabilization and mesh refinement. In an additional study, we have confirmed the findings of [22] that in the absence of diffusion ($\kappa = 0$), an initial condition with a jump can be traced *exactly* by means of a step-enriched space-time XFEM approximation.

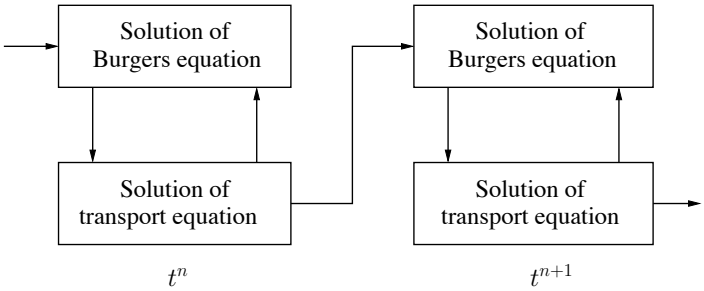

Figure 8. Strong coupling loop of the Burgers equation and the transport equation for the level-set function.

4.5.3. Burgers equation with moving high gradient (position not known) The third test case is a convection-dominated Burgers equation like the first test case in section 4.5.1 but this time, instead of using a symmetric initial condition, an asymmetric initial condition is used. That is,

$$u_0(x) = . \begin{cases} -2\sin\pi(x) & \text{for } \phi_0(x) \leqslant 0 \ , \\ -0.2\sin\pi(x) & \text{for } \phi_0(x) > 0 \ . \end{cases} \tag{4.10}$$

As a result, the position of the high gradient is now moving in time. This movement in time is non-linear due to the non-linearity in the transport term of the Burgers equation. Only the initial position of the high gradient is given and described through $\phi_0(x) = x$. As in the previous test case, the movement of the highest gradient in time is captured by solving a transport problem for ϕ. Other test case parameters are specified as $\Omega =]-1, 1[$, $\kappa = 5 \times 10^{-3}$ and $T = 0.3$.

It is important to note the mutual dependence of the Burgers equation for u and the transport equation for ϕ. On the one hand, the result of the Burgers equation u effects the advection velocity of the transport equation for ϕ. On the other hand, the zero-level of ϕ defines the position of the largest gradient in the enrichment functions, so that the approximation space of the Burgers equation is effected by ϕ. The mutual dependence of u and ϕ leads to a coupled problem in the sense of Felippa and Park [23, 24]. Here, we solve the coupled problem by a strong coupling loop of the two fields within each of the 80 time steps, see Figure 8.

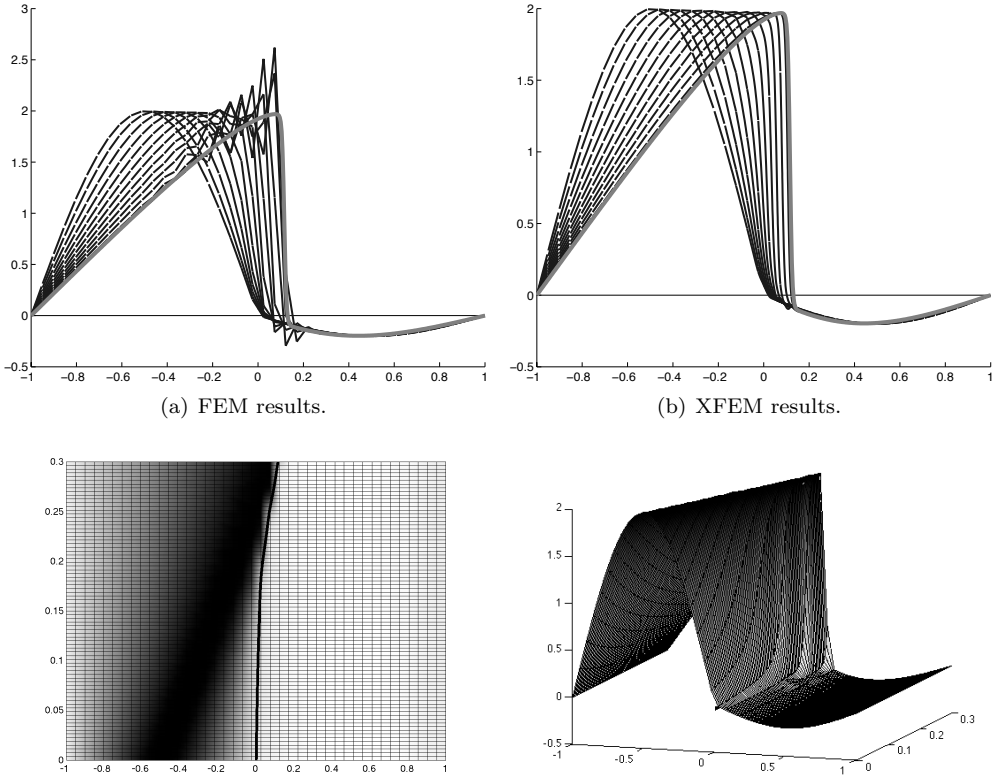

(a) FEM results.

(b) XFEM results.

(c) XFEM results in the space-time domain.

(d) XFEM results in the space-time domain.

Figure 9. Unstabilized results for the Burgers equation.

The unstabilized solution for the FEM is shown in Figure 9(a) and large oscillations are observed. In comparison, the XFEM solution 9(b) shows no oscillations. A space-time view of the problem is shown in figure 9(c) where the curved line represents the zero level of the level-

set function and is the position of the highest gradient. This figure shows the non-linearity in the position of the highest gradient over time.

We conclude that the non-linear movement of the high gradient can be captured well so that the enrichment scheme stays effective throughout the simulation.

4.5.4. Advection-diffusion equation in two dimensions The fourth test case is an instationary, linear advection-diffusion problem in two dimensions where a scalar function is tranported in a circular velocity field. That is, the components of the velocity $\boldsymbol{c}$ are given as

$$c_x = y - 0.5 \qquad \text{and} \qquad c_y = -x + 0.5. \tag{4.11}$$

The initial condition u_0 is specified by (4.3) with $\epsilon = 0.19h$, where h is the mesh size. This initial condition involves locally very high gradients but is constant in the major part of the domain. Other test case parameters are specified as $\Omega =]0, 1[$, $\kappa = 10^{-6}$ and $T = 1$.

A square mesh of 31×31 elements is used. For brevity, only the XFEM results are shown in figure 10. No oscillations are observed for a rotation of the initial condition of 150° which is realized in 200 time-steps. The three figures 10(a) to (c) show the approximation at the integration points after 1, 100 and 200 time steps, respectively. No oscillations are seen without any smoothing of the high gradient. The proposed enrichment scheme obviously extends straightforward to more than one spatial dimension.

5. XFEM for high gradients at the boundary (boundary layers)

Standard finite element approximations without stabilization also result into oscillatory solutions for high gradients near the boundary (boundary layers). Typical meshes in fluid mechanics are highly refined near the boundary as these regions have an important influence in the ability of the approximation to capture the physics of a flow problem properly. Again, the aim is to define enrichment funtions for XFEM approximations that are able to obtain highly accurate solutions without stabilization and mesh refinement. For a prescribed level of accuracy, a drastical decrease in the number of degrees of freedom is then expected for XFEM simulations compared to FEM simulations on refined meshes near the boundary.

In many applications, boundary layers are not present along the whole boundary Γ of the domain, for example, typically not at slip boundaries or at the inflow and outflow. The enrichment is therefore only desired along selected parts of the boundary which is labelled $\Gamma_{\text{enr}} \subseteq \Gamma$. This is often the part of the boundary where no-slip boundary conditions are applied.

An important difference to the situation considered in the previous section is that the position of the highest gradient is now the boundary itself, so that the level-set method is *not* needed for the definition of the enrichment functions. Instead, the enrichment functions should depend on the discretization near the wall. They are only mesh-dependent, i.e. the parameters of the governing equations are not used. A different strategy would be to employ only one enrichment function and estimate the thickness of the boundary layer, e.g. in an iterative procedure. It is noted that, as long as the boundaries are fixed in space, the enrichment functions for boundary layers are time-independent.

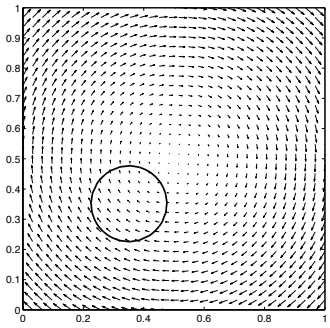

(a) Prescribed velocity field.

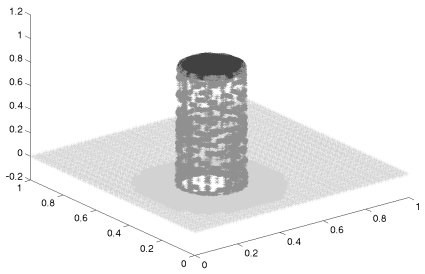

(b) Solution at $t = 1$.

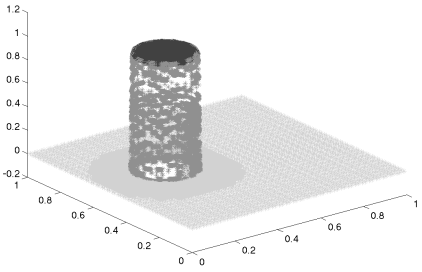

(c) Solution at $t = 100$.

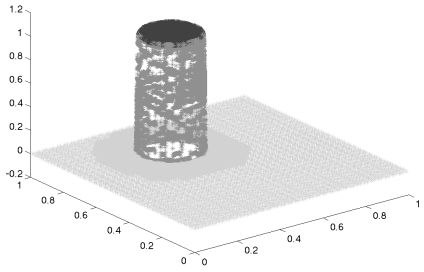

(d) Solution at $t = 200$.

Figure 10. Unstabilized XFEM results for the linear advection-diffusion equation in two dimensions. The high-gradient solution is plotted at the integration points in the domain.

5.1. Optimal set of enrichment functions

We again start by finding an "optimal" set of enrichment functions. A similar procedure as described in section 4.2 is employed. The domain is again $\Omega =]0, 1[$ and the different functions for $f(x)$ have high gradients at $x = 1$. We use functions $f(x)$ of the kind x^q, $\exp(q \cdot x)$, and $\sinh(q \cdot x)$, where the parameter $q \gg 1 \in \mathbb{R}$ scales the gradient. The set of m enrichment functions is based on

$$\psi(\boldsymbol{x}, L) = \frac{\exp(q \cdot S_L(\boldsymbol{x}) - 1)}{\exp(q) - 1} \tag{5.1}$$

Enrichment Function	q	Layer L
ψ_1	50	1
ψ_2	15	1
ψ_3	12	2
ψ_4	10	3

Table II. The set of 4 enrichment functions used for high gradients near the wall.

The function $S_L(\boldsymbol{x})$ varies between 0 and 1 within L element layers of the wall for $L = 1, 2, 3$. They are defined by means of standard finite element shape functions:

$$S_1(\boldsymbol{x}) = \sum_{i \in J_1} N_i(\boldsymbol{x}), \tag{5.2}$$

$$S_2(\boldsymbol{x}) = \frac{1}{2}\Big(\sum_{i \in J_2} N_i(\boldsymbol{x}) + 2 \cdot \sum_{i \in J_1} N_i(\boldsymbol{x}) \Big), \tag{5.3}$$

$$S_3(\boldsymbol{x}) = \frac{1}{3}\Big(\sum_{i \in J_3} N_i(\boldsymbol{x}) + 2 \cdot \sum_{i \in J_2} N_i(\boldsymbol{x}) + 3 \cdot \sum_{i \in J_1} N_i(\boldsymbol{x}) \Big). \tag{5.4}$$

The nodal set J_1 is built by the nodes along the enriched boundary Γ_{enr}, J_2 are the nodes one element layer away from Γ_{enr}, and J_3 are the nodes two element layers away from Γ_{enr}. The situation is depicted in Figure 11 in one and two dimensions.

The optimal set for 4 enrichment functions is given in table II. These enrichment functions are visualized in two dimensions in Figure 12. For high gradients near boundaries, we find that using more enrichment functions does not improve the results noticeable. It is not sufficient to enrich only the nodes in the first element layer next to Γ_{enr}, i.e. in this case, oscillations in the approximated solution remain. Higher gradients than the one defined through ψ_1 require a very large number of integration points in the enriched elements and affect the conditioning of the system of equations unfavorably.

5.2. Quadrature

The high gradients in the enrichment functions require an accurate quadrature. Because the highest gradient is present near the boundary and thus aligns with the element edges, no decomposition into subelements for integration purposes is required. Therefore, we use standard Gauss rules with a large number of integration points in the enriched elements. The integration points are then concentrated near the element edges where they are needed.

5.3. Numerical examples with high gradients at the boundary

Three stationary convection-dominated problems are considered. The optimal set of four enrichment functions described in section 5.1 is used to enrich the approximation space. The position of the highest gradient is on the boundary Γ_{enr} which is enriched.

5.3.1. Advection-diffusion equation in one dimension The stationary advection-diffusion equation in one dimension is considered first, the governing equations of section 3.1 are modified accordingly. The domain is $\Omega =]0, 1[$ with boundary conditions $u(0) = 0$ and $u(1) = 1$. The

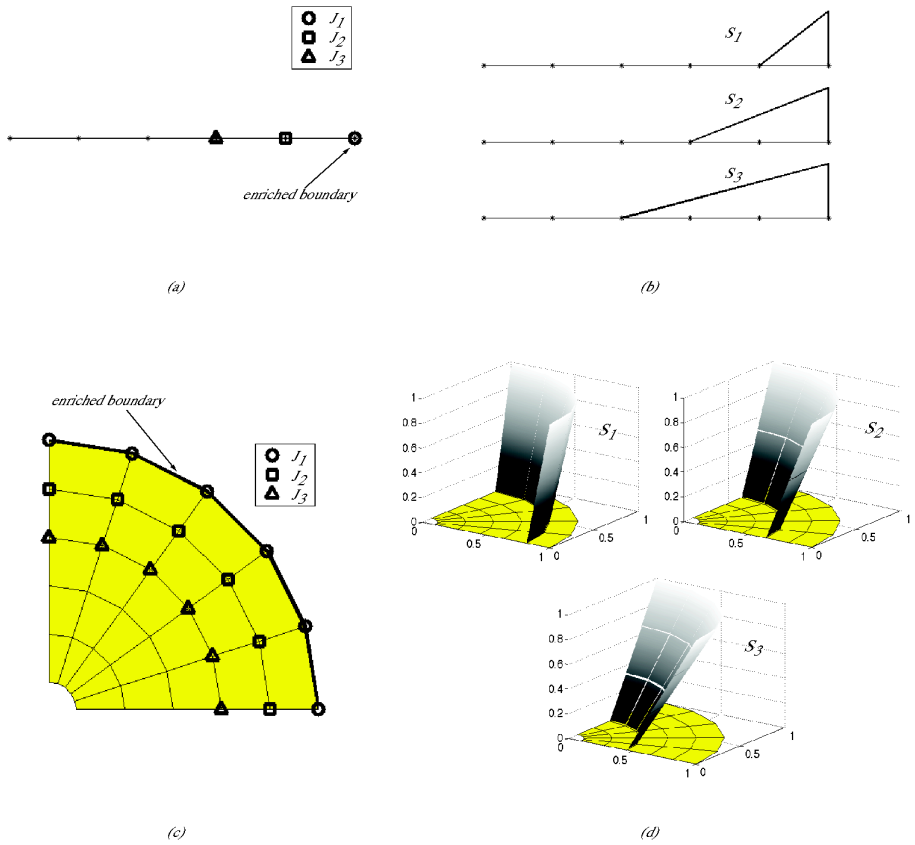

Figure 11. The functions S_L and nodal sets J_L in one and two dimensions. Note that each function S_L extends over L element layers near the enriched boundary.

exact solution is

$$u^{ex}(x) = \frac{\exp(c/K \cdot x) - 1}{\exp(c/K - 1)}. \tag{5.5}$$

Three different ratios c/K are considered: $c/K = \{1, 20, 40\}$ leading to a small, moderate, and high gradient at $x = 1$, see Figure 13. The number of linear elements n is varied from $10, 20, \ldots, 640$. The error in the L_2-norm for the three different c/K-ratios is shown in Figure 14(a) for unstabilized XFEM and FEM results. For $c/K = 1$, the FEM and XFEM results are very similar over the whole range of elements. This shows that, as expected, the enrichment is not needed for this case. For $c/K = 20$ and $c/K = 40$, on coarse meshes, the XFEM-results are drastically improved compared to the FEM results. For finer meshes, the XFEM results converge to the FEM solution as the enrichment becomes less useful.

The largest pointwise error in the domain (maximum oscillation) over the whole range of $c/K \in]0, 500[$ for three different numbers of elements $n = \{10, 40, 160\}$ is studied in Figure 14(b). It is seen that for the XFEM approximation no oscillations are observed up to $c/K = 500$

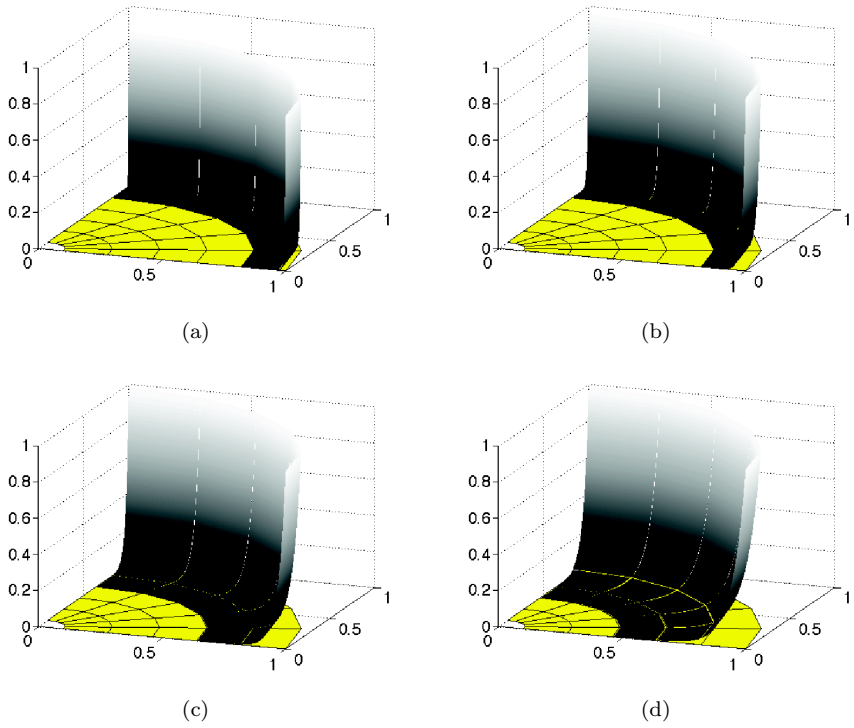

Figure 12. The resulting 4 enrichment functions in two dimensions for the domain shown in Figure 11(c).

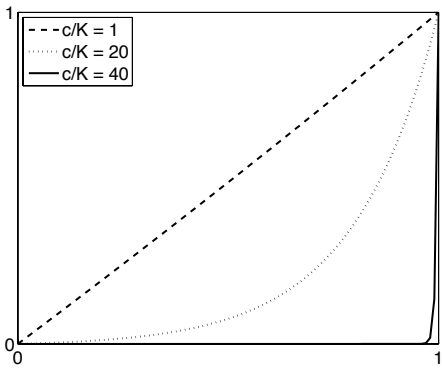

Figure 13. The exact solutions for $c/K = \{1, 20, 40\}$ leading to a small, moderate, and high gradient at $x = 1$, respectively.

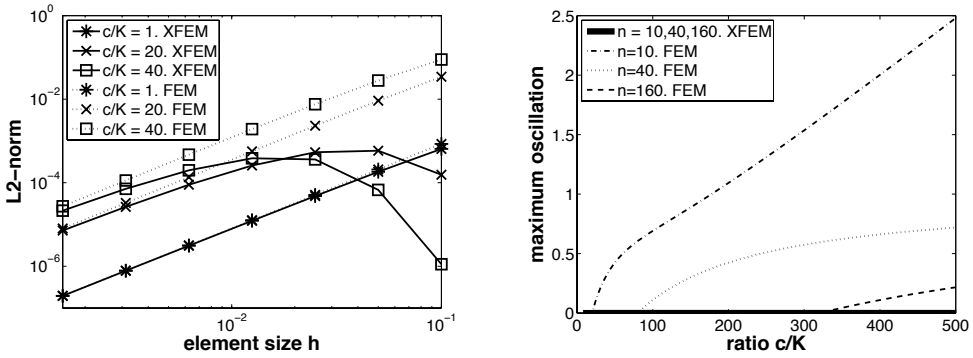

(a) (b)

Figure 14. (a) Convergence in the L_2-norm, (b) largest pointwise error (maximum oscillation) for XFEM and FEM approximations.

even on the coarsest mesh. In contrast, the unstabilized FEM shows large pointwise errors that increase with c/K. It is thus seen that the proposed set of enrichment functions produces highly accurate results over the complete range of high gradients near the boundary.

5.3.2. Burgers equation in one dimension A similar study is repeated for the stationary Burgers equation in one dimension. The domain is $\Omega =]-1, 0[$ and the exact solution is given as

$$u^{ex}(x) = -2\kappa s \cdot \frac{\exp(2sx) - t}{\exp(2sx) + t} \qquad \text{with } s, t \in \mathbb{R}. \tag{5.6}$$

The Dirichlet boundary conditions are chosen such that Equation (5.6) is the exact solution with $s = 20, t = 1$, see Figure 15(a). The diffusion parameter is set to $\kappa = 10^{-3}$.

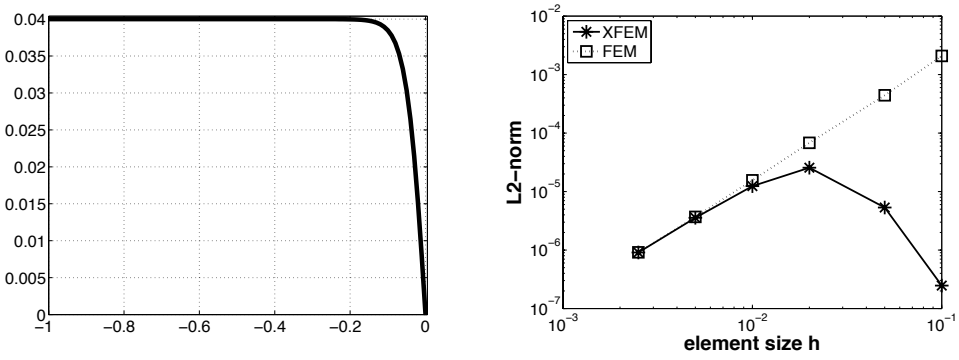

(a) (b)

Figure 15. (a) The exact solution of the Burgers equation for $\kappa = 0.001, s = 20, t = 1$, (b) convergence in the L_2-norm for XFEM and FEM approximations.

Convergence results in the L_2-norm are shown in Figure 15(b) for unstabilized XFEM and FEM approximations. The findings of the previous section are confirmed: On coarse meshes the situation improves drastically with the extended approximation. We have also investigated different gradients at $x = 0$ and studied the maximum pointwise error. These results are omitted for brevity as they are very similar to the ones obtained in the previous test-case and lead to the same conclusions.

5.3.3. Advection-diffusion equation in two dimensions As a third text-case, the stationary advection-diffusion equation in two dimensions is considered. The domain Ω is a 90° segment spanned by $r_1 = 0.1$ and $r_2 = 1.0$ and is shown in Figure 16(a). The exact solution is

$$u^{ex}(x, y) = \frac{\exp(c_x/K \cdot x + c_y/K \cdot y) - 1}{\exp(c_x/K + c_y/K) - 1}. \tag{5.7}$$

The boundary conditions are applied along Γ accordingly. The gradient at $\Gamma_{\text{enr}} = \{\boldsymbol{x} : \|\boldsymbol{x}\| = r_2\}$, where $\|\cdot\|$ is the Euclidean norm, is scaled by the ratios of c_x/K and c_y/K. We choose $c_x = c_y = c$ in this test case. The exact solution for $c/K = 5$ is shown in Figure 16(b). It is important to note that the solution involves a high gradients in normal direction to the wall but only changes mildly along Γ_{enr}. A typical opimized mesh for standard FEM computations would consist of high-aspects ratio elements along the boundary in order to resolve the boundary layer. However, for the computations considered in this work, the element size in normal direction is constant.

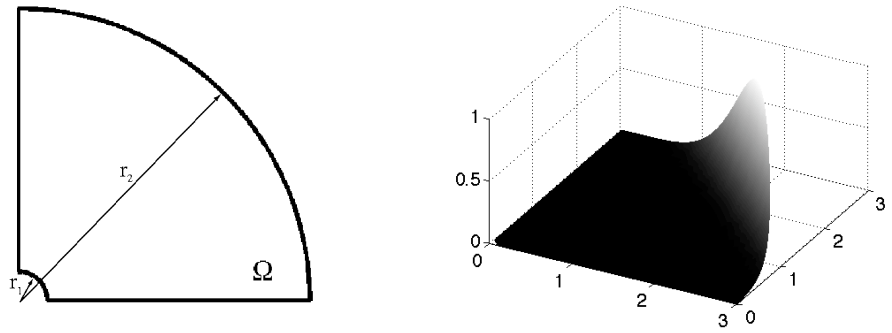

(a) (b)

Figure 16. (a) The domain Ω, (b) the exact solution of the advection-diffusion problem for $c/K = 5$.

A convergence study is carried out comparing the proposed set of enrichment functions with a standard FE approximation. In Fig. 17(a), for varying element numbers, the errors are shown in the L_2-norm for different $c/k = \{5, 20, 100\}$. Our findings in one dimensions are again confirmed for this two-dimensional test case: On coarse meshes the accuracy is largely improved for the XFEM, on finer meshes, XFEM and FEM results converge to each other. As an example, for $c/K = 200$, the same level of accuracy than the XFEM results on a 10×10 mesh is obtained for the FEM with a uniformly refined mesh of 80×80 elements.

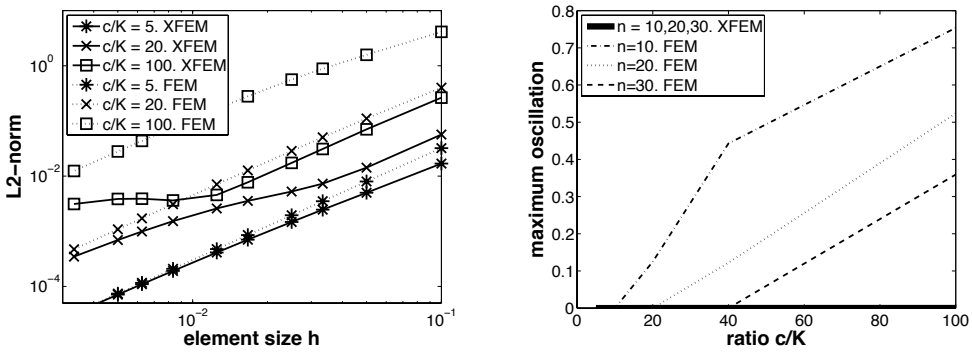

(a) (b)

Figure 17. (a) Convergence in the L_2-norm, (b) largest pointwise error (maximum oscillation) for XFEM and FEM approximations.

The largest pointwise error (maximum oscillation) is studied again. For different meshes with 10×10, 20×20, and 30×30 elements the ratio c/K is varied in the range from 0 to 100, see Figure 17(b). As expected the FEM results worsen with increasing c/K ratio. The XFEM results show again no visible oscillations. It is thus seen that although the enrichment functions ψ_1 to ψ_4 are constant in tangential direction of Γ_{enr}, see Figure 12, the XFEM approximation is able to capture both, the large gradient in normal direction and the moderate change in tangential direction of Γ_{enr}.

6. Conclusions

An enrichment scheme for the XFEM has been proposed which enables highly accurate approximations of convection-dominated problems without stabilization or mesh refinement. The high gradients inside the domain (shocks) and at the boundary (boundary layers) are captured by a set of enrichment functions used in the vicinity of the high gradients.

For high gradients in the domain, the enrichment functions are regularized step functions that depend on the distance from the shock. The position of the highest gradient is described by the level-set function. Moving shocks are considered for by solving an additional advection problem for the level-set function. For high gradients at the boundary, exponential functions are used as enrichment functions. They depend on the discretization along the boundary and no level-set function is needed. The enrichment for boundary layers is independent of time as long as the boundary is fixed.

The proposed enrichment scheme is independent of parameters in the governing equations. The whole set of enrichment functions was used in all test-cases, i.e. no iterative procedure is needed in each time-step in order to determine only *one* suitable enrichment function.

The next step is to apply the proposed enrichment scheme to flow problems which are convection-dominated in many problems of practical relevance. The results will be reported in a forthcoming publication.

ACKNOWLEDGEMENTS

Financial support from the Deutsche Forschungsgemeinschaft (German Research Association) through grant GSC 111 and the Emmy-Noether program is gratefully acknowledged.

REFERENCES

1. Belytschko T, Black T. Elastic crack growth in finite elements with minimal remeshing. *Internat. J. Numer. Methods Engrg.* 1999; **45**:601 – 620.
2. Moës N, Dolbow J, Belytschko T. A finite element method for crack growth without remeshing. *Internat. J. Numer. Methods Engrg.* 1999; **46**:131 – 150.
3. Elguedj T, Gravouil A, Combescure A. Appropriate extended functions for X-FEM simulation of plastic fracture mechanics. *Comp. Methods Appl. Mech. Engrg.* 2006; **195**:501 – 515.
4. Gravouil A, Moës N, Belytschko T. Non-planar 3D crack growth by the extended finite element and level sets, part II: level set update. *Internat. J. Numer. Methods Engrg.* 2002; **53**:2569 – 2586.
5. Moës N, Gravouil A, Belytschko T. Non-planar 3D crack growth by the extended finite element and level sets, part I: mechanical model. *Internat. J. Numer. Methods Engrg.* 2002; **53**:2549 – 2568.
6. Karihaloo B, Xiao Q. Modelling of stationary and growing cracks in FE framework without remeshing: a state-of-the-art review. *Computers & Structures* 2003; **81**:119 – 129.
7. Brooks A, Hughes T. Streamline upwind/Petrov-Galerkin formulations for convection dominated flows with particular emphasis on the incompressible Navier-Stokes equations. *Comp. Methods Appl. Mech. Engrg.* 1982; **32**:199 – 259.
8. Hughes T, Franca L, Hulbert G. A new finite element formulation for computational fluid dynamics: VIII. The Galerkin/least-squares method for advective-diffusive equations. *Comp. Methods Appl. Mech. Engrg.* 1989; **73**:173 – 189.
9. Donea J, Huerta A. *Finite Element Methods for Flow Problems*. John Wiley & Sons: Chichester, 2003.
10. Patzák B, Jirásek M. Process zone resolution by extended finite elements. *Eng. Fract. Mech.* 2003; **70**:957 – 977.
11. Areias P, Belytschko T. Two-scale method for shear bands: thermal effects and variable bandwidth. *Internat. J. Numer. Methods Engrg.* 2007; **72**:658 – 696.
12. Benvenuti E. A regularized XFEM framework for embedded cohesive interfaces. *Comp. Methods Appl. Mech. Engrg.* 2008; **197**:4367 – 4378.
13. Waisman H, Belytschko T. Parametric enrichment adaptivity by the extended finite element method. *Internat. J. Numer. Methods Engrg.* 2008; **73**:1671 – 1692.
14. Osher S, Fedkiw R. *Level Set Methods and Dynamic Implicit Surfaces*. Springer Verlag: Berlin, 2003.
15. Sethian J. *Level Set Methods and Fast Marching Methods*. 2 edn., Cambridge University Press: Cambridge, 1999.
16. Tezduyar T, Sathe S. Stabilization parameters in SUPG and PSPG formulations. *J. Comput. Appl. Math.* 2003; **4**:71 – 88.
17. Benvenuti E, Tralli A, Ventura G. A regularized XFEM model for the transition from continuous to discontinuous displacements. *Internat. J. Numer. Methods Engrg.* 2008; **74**:911 – 944.
18. Xiao Q, Karihaloo B. Improving the accuracy of XFEM crack tip fields using higher order quadrature and statically admissible stress recovery. *Internat. J. Numer. Methods Engrg.* 2006; **66**:1378 – 1410.
19. Bordas S, Nguyen P, Dunant C, Guidoum A, Nguyen-Dang H. An extended finite element library. *Internat. J. Numer. Methods Engrg.* 2007; **71**:703 – 732.
20. Daux C, Moës N, Dolbow J, Sukumar N, Belytschko T. Arbitrary branched and intersecting cracks with the extended finite element method. *Internat. J. Numer. Methods Engrg.* 2000; **48**:1741 – 1760.
21. Fries T, Zilian A. On time integration in the XFEM. *Internat. J. Numer. Methods Engrg.* 2009; **79**:69 – 93.
22. Chessa J, Belytschko T. Arbitrary discontinuities in space-time finite elements by level-sets and X-FEM. *Internat. J. Numer. Methods Engrg.* 2004; **61**:2595 – 2614.
23. Park K, Felippa C, Ohayon R. Partitioned formulation of internal fluid-structure interaction problems by localized lagrange multipliers. *Comp. Methods Appl. Mech. Engrg.* 2001; **190**:2989 – 3007.
24. Felippa C, Park K, Farhat C. Partitioned analysis of coupled mechanical systems. *Comp. Methods Appl. Mech. Engrg.* 2001; **190**:3247 – 3270.